DSTO

# Effect of Plate Thickness on the In-Plane and Through-Thickness Stresses at a Hole

R.L. Evans



DEPARTMENT OF DEFENCE

DEFENCE SCIENCE AND TECHNOLOGY ORGANISATION

# Effect of Plate Thickness on the In-Plane and Through-Thickness Stresses at a Hole

*R.L. Evans*

**Airframes and Engines Division**
**Aeronautical and Maritime Research Laboratory**

DSTO-TR-0330

**ABSTRACT**

A combined experimental and numerical study has been carried out to examine the influence of thickness on the surface and through-thickness stress distributions of aluminium alloy specimens with central holes. Thermographic and strain-gauge measurements were made on several thicknesses of specimens, the central holes of which were either reamed or cold-expanded by 3.6%. The experimental results were compared with those from numerical analyses of the specimens by three-dimensional finite-element modelling.



**RELEASE LIMITATION**

*Approved for public release*

DEPARTMENT OF DEFENCE

DEFENCE SCIENCE AND TECHNOLOGY ORGANISATION

*Published by*

*DSTO Aeronautical and Maritime Research Laboratory*
*PO Box 4331*
*Melbourne Victoria 3001*

*Telephone: (03) 9626 8111*
*Fax: (03) 9626 8999*

*AR No. AR-009-683*
*April 1996*

**APPROVED FOR PUBLIC RELEASE**

# Effect of Plate Thickness on the In-Plane and Through-Thickness Stresses at a Hole

## Executive Summary

Holes exist in metallic aircraft structures for either design or construction reasons and their stress concentrating effect is such that they are common regions of fatigue crack initiation.

Theoretical studies have indicated that the stress concentration factor (maximum local stress/remote stress) of a hole varies through the thickness of a plate and is sensitive to the value of hole diameter to plate thickness ratio (D/t), and to Poisson's ratio. Theory has also shown that the assumption of plane stress is adequate for thin plates which have a thickness less than one quarter the hole diameter. For thick plates—which have a thickness of at least twice the diameter of the hole—the three-dimensional stress concentration factor should be used.

To assess the validity of the various solutions, an experimental study, including thermoelastic and strain-gauge measurements, has been carried out at AMRL. This report presents the results of the study which examined the influence of plate thickness on the three-dimensional stress distribution of aluminium alloy specimens with central holes. The variations in surface stresses and through-the-thickness stresses, with specimens of thickness 10, 20 or 35 mm, have been investigated. Three-dimensional elastic finite-element analyses were also conducted.

The experimental data compared well with the numerical finite-element work for the surface of the specimens. The corresponding through-thickness data were not as clearly in accordance, due to experimental problems. The numerical finite-element work undertaken in this report validates the trends of other published finite-element and analytical studies, that as the thickness of a plate with a hole increases, the maximum stress concentration factor, which is in the middle of the plate, increases and the minimum value of stress concentration factor, which is at the surface of the plate, decreases. It is shown that caution must be taken in engineering calculations for thick plates with holes—the common use of a two-dimensional handbook stress concentration factor may be too conservative at the surface, but unconservative at mid-thickness.

# Author

**Rebecca Evans**
Airframes and Engines Division

*Rebecca Evans completed a Bachelor of Engineering in Aeronautical Engineering at the Royal Melbourne Institute of Technology in 1987. In 1988 she commenced work in Systems Division at DSTO Salisbury, where she worked on the design, analysis and testing of towed targets. Since 1992 she has been working in the Airframes and Engines Division where she has undertaken experimental and finite-element analyses of metallic aircraft components, evaluating various fatigue life enhancement techniques.*

# Contents

# Notation

| | |
|---|---|
| D | Hole diameter (mm) |
| E | Young's modulus (MPa) |
| H | Specimen height (mm) |
| $K_t$ | Elastic stress concentration factor = $(\sigma_y/\sigma_o)$ |
| W | Specimen width (mm) |
| k | Calibration factor |
| r | Hole radius (mm) |
| t | Specimen thickness (mm) |
| $\varepsilon_x$, $\varepsilon_y$, $\varepsilon_z$ | Normal strain in the x, y and z directions, respectively |
| $\nu$ | Poisson's ratio |
| $\sigma_{bulk}$ | Bulk stress $(\sigma_x + \sigma_y + \sigma_z)$ (MPa) |
| $\sigma_o$ | Applied gross-area stress (MPa) |
| $\sigma_x$, $\sigma_y$, $\sigma_z$ | Normal stress in the x, y and z directions, respectively (MPa) |

# Abbreviations

| | |
|---|---|
| CE | Cold-Expanded |
| FAST | Focal-plane Array for Synchronous Thermography |
| NCE | Non-Cold-Expanded |
| PAFEC | Program for Automatic Finite Element Calculations |
| SCF | Stress Concentration Factor |
| SD | Standard Deviation |
| SPATE | Stress Pattern Analysis by the measurement of Thermal Emission |

# 1. Introduction

Recent work relevant to the assessment of structural integrity of aircraft has considered the influence of three-dimensional stresses at holes. Several papers have presented analytical solutions for the three-dimensional stress field at a hole in a large plate of arbitrary thickness; [1-5] being a selection. Historical summaries of this subject can be found in papers by Folias and Wang [1], and Youngdahl and Sternberg [2]. In the analytical papers the plate is assumed to be of a homogeneous, isotropic, elastic material, to be infinite in width and height, and have a remote tensile stress applied. These studies have shown that the stress concentration factor varies through the thickness of the plate and is sensitive to the ratio of hole diameter to plate thickness ($D/t$) and Poisson's ratio ($\nu$), and that the Young's modulus of the material has no effect on the value of the factor. Other findings are; that the assumption of plane stress is adequate for ratios of $D/t \geq 4$, and for ratios of $D/t \leq 0.5$ the three-dimensional stress concentration factor should be used.

A finite-element study on this problem has been presented by Shivakumar and Newman [6]. As in the analytical studies, the plate was assumed to be of a homogeneous, isotropic, elastic material, however, the plate was finite in width and height. Several load cases were covered (tension, bending and pin-loading), and both straight and countersunk holes were considered. (It should be noted that in the course of this present study, an error was discovered in this paper. The figures and text mention that the plate (with a straight-shank hole) has a height and width of 5 times the diameter of the hole, whereas the height and width are equal to 10 times the hole diameter. The authors have confirmed this error and a subsequent ESDU data sheet (93030) based on [6] is to be amended.)

These several studies [1-6] do not appear to be associated with any confirmatory experimental program. To validate the various numerical solutions, an experimental study has now been carried out at AMRL which examines the influence of plate thickness on the three-dimensional stress distribution of aluminium alloy specimens with central holes. The variations in surface stresses and through-the-thickness stresses, with specimens of thickness 10, 20 or 35 mm, have been investigated. The stress distribution in the specimens, which each had a reamed-only or a cold-expanded central hole of diameter 22.6 mm, was obtained via thermographic measurements taken by a system called FAST (Focal-plane Array for Synchronous Thermography) [7]. Some of the specimens also had strain-gauge measurements taken. Three-dimensional elastic finite-element analyses were conducted for calibration of the thermographic data, and for comparison with the strain-gauge data and previous analytical work.

# 2. Theoretical Analyses

The main consideration of the analytical papers is the variation in stress concentration factor ($\sigma_y/\sigma_o = K_t$) through the thickness of the specimen. However the variation in ($\sigma_z/\sigma_o$) through the thickness of the specimen is also required to enable comparison with, and calibration of, the experimental FAST data which are output in digital levels that range from -128 to 127. Three of the papers referenced above have determined the $\sigma_z$ component, however they did not consider two of the important conditions in the present examination, namely, a plate and hole of finite dimensions, and $\nu = 0.33$ (for aluminium). The strain-gauge locations for the experimental stress determinations were unsuitable for calibrating FAST, hence finite-element analyses were undertaken with the added benefit of determining stresses for the exact material and geometry under consideration. These three-dimensional elastic finite-element (FE) stress analyses were undertaken using the PAFEC suite of programs, level 8.1, run on a HP9000-755 computer.

## 2.1 Comparison with Published Results for a Circular Hole in a Large Plate

Two additional FE analyses were undertaken to give confidence in the modelling method used; one to compare with the corrected numerical study of [6], and the other to compare with Folias and Wang's analytical work on an infinite plate [1].

### 2.1.1 Numerical Study

The geometry and material properties of the PAFEC model were identical to one of the cases studied in [6]. The plate which was under a tensile load, had a height and width of 10D, that is, ten times the hole diameter (refer to Fig. 1 for axis and dimension notation) and $\nu = 0.3$, and a similar mesh to that in [6] was used. The PAFEC stress concentration factors ($K_t$) for the selected case of D/t=2 were between 0.28% and 0.65% lower than those reported in [6]. Several verifications of the FE analysis were completed and it was concluded that the model was suitably accurate. As an independent check, the same case was repeated with the NASTRAN FE package; version 68.1.0, November 15 1994, run on an IBM RISC System-6000, [8]. A similar mesh to the PAFEC model was used and the $K_t$ values for the comparison with [6] were less than 0.15% higher than the corresponding PAFEC results, refer to Table 1.

*Table 1. Comparison of values of SCF as determined by various FE programs for D/t=2 and W=H=10D*

| z/t | Stress Concentration Factor | | | \| % Difference \| | | |
|---|---|---|---|---|---|---|
| | Ref. [6] | PAFEC | NASTRAN | Ref. [6] & PAFEC | Ref. [6] & NASTRAN | PAFEC & NASTRAN |
| 0 | 3.2 | 3.191 | 3.195 | 0.281 | 0.156 | 0.125 |
| 0.5 | 2.94 | 2.921 | 2.925 | 0.646 | 0.510 | 0.137 |

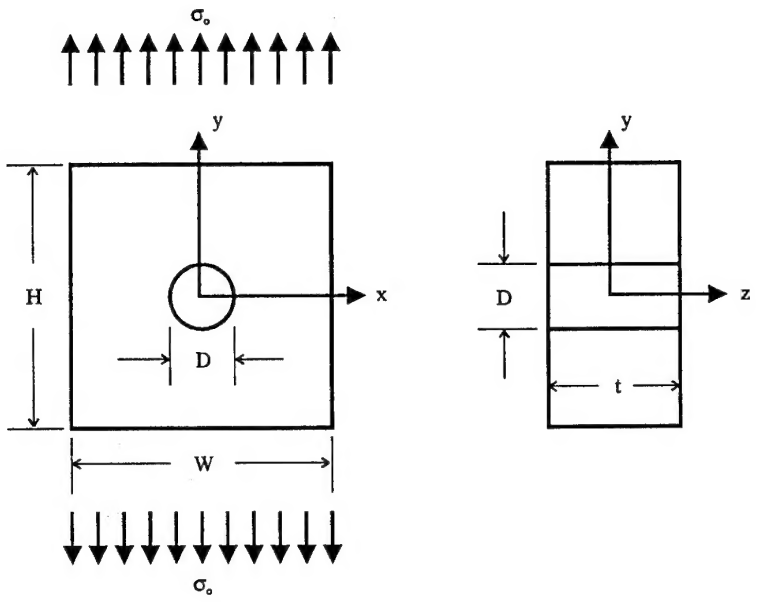


(a) View of specimen surface (b) Section through y-z plane

*Figure 1. Axis and notation for circular hole in a plate*

### 2.1.2 Analytical Study

The infinite plate case examined analytically by Folias and Wang where D/t = 2 was modelled by the same large plate geometry of section 2.1.1 (ie, height and width equal to 10D) with $\nu = 0.33$. The PAFEC $K_t$ values for this case (of D/t = 2) were on average 2.7% higher than those reported in [1]. Again an independent check was made by repeating the comparison using the NASTRAN FE package. NASTRAN gave $K_t$ values which were less than 0.14% higher than the corresponding PAFEC results (refer to Table 2) hence, any difference between the PAFEC and NASTRAN models is negligible. Part of the discrepancy between the analytical and numerical "infinite" plate could be attributed to the finite width effect (assessed as ≈1.3% from [9]). The balance of the difference (≈1.4%) can readily be attributed to the finite height, numerical error of the FE package, the accuracy of [1], or a combination of the three.

*Table 2. Comparison of values of SCF as determined by analytical and FE models for D/t=2, and W=H=10D for FE models*

| z/t | Stress Concentration Factor | | | \| % Difference \| | | |
|---|---|---|---|---|---|---|
| | Ref. [1] | PAFEC | NASTRAN | Ref. [1] & PAFEC | Ref. [1] & NASTRAN | PAFEC & NASTRAN |
| 0 | 3.1 | 3.191 | 3.195 | 2.935 | 3.065 | 0.125 |
| 0.5 | 2.85 | 2.921 | 2.925 | 2.491 | 2.632 | 0.137 |

## 2.2 Numerical Analysis of Test Specimens

The three non-cold-expanded experimental specimens, Fig. 2, were modelled using 20-noded isoparametric solid-brick elements. The mesh of the model of the 10 mm thick specimen is shown in Fig. 3 and is comprised of 2513 elements. The PAFEC data file for this model is listed in Appendix A. Due to symmetry, only one-eighth of the structure was modelled. The meshes for the 20 mm and the 35 mm thick specimens were comprised of 4308 and 4185 elements, respectively. Appropriate boundary condition constraints were placed at all planes of symmetry. A remote stress of 30 MPa was applied to the x-z plane at a location corresponding to the placement of the fatigue machine grips on the specimen, as schematically depicted in Fig. 2. The data obtained from these analyses included bulk-stress values on the surface and down the bore of the hole as appropriate to compare with experimental readings.

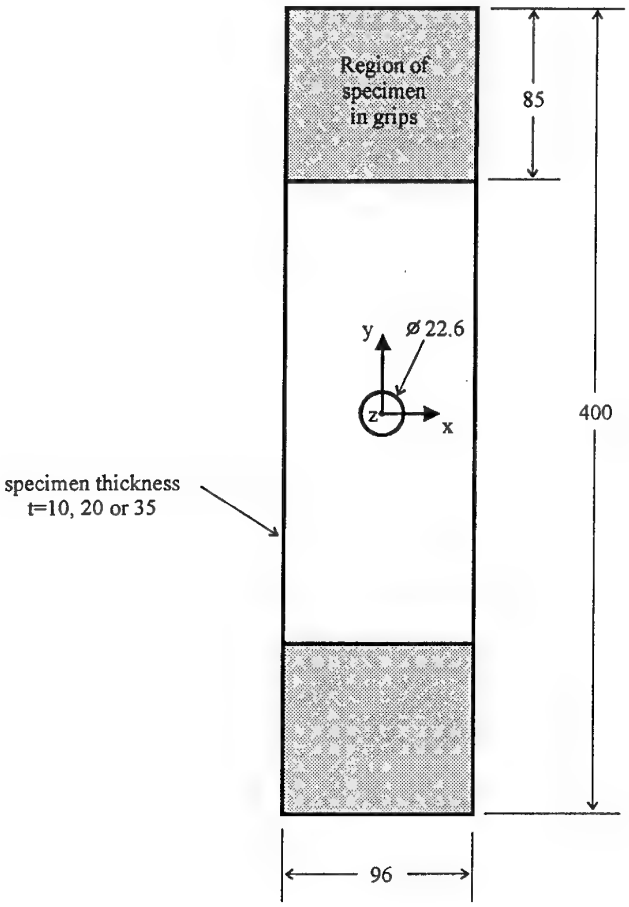


*Figure 2. Geometry of specimens (Dimensions in mm)*

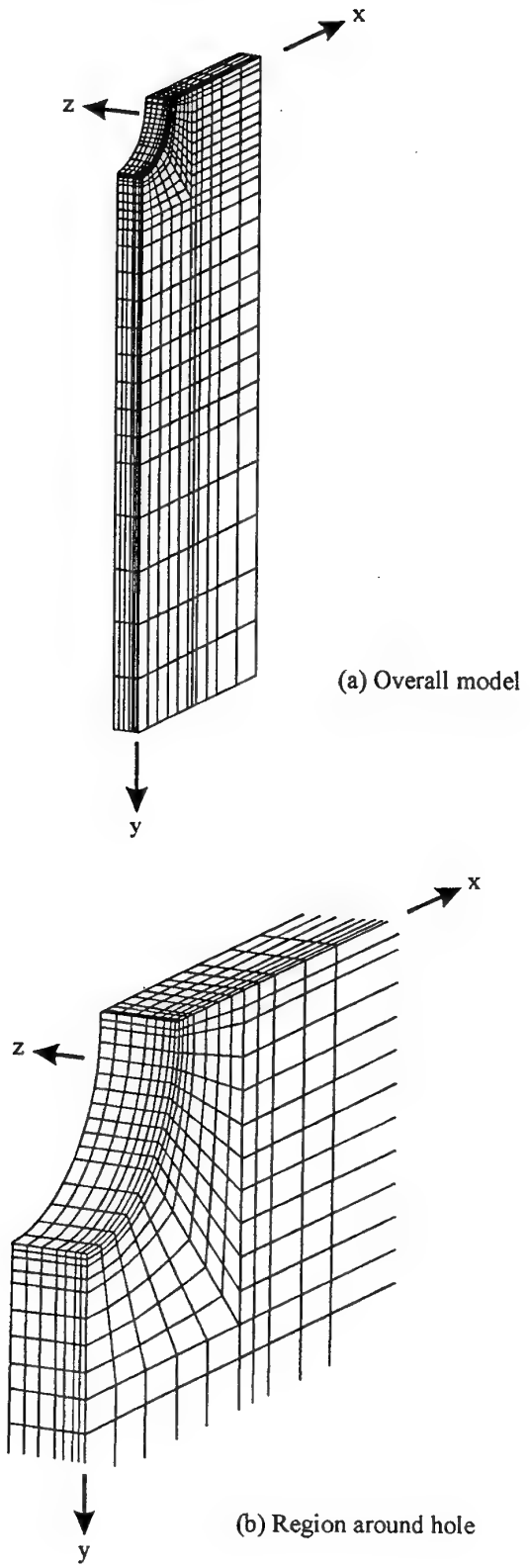


*Figure 3. Finite element mesh for 10 mm thick specimen*

# 3. Experimental Analyses

## 3.1 Specimen Details

The six specimens used in this investigation were manufactured from 45 mm thick rolled plates of 2214–T651 aluminium alloy and consisted of a rectangular plate with a centrally located hole. The specimen configuration is shown in Fig. 2, and the specimens have constant thicknesses of either 10, 20 or 35 mm (two of each thickness). The central hole in half of the specimens, one of each thickness, was cold-expanded (CE) by 3.6% (using the Boeing split-sleeve system as discussed in [10]) and then lightly reamed to 22.6 mm diameter. The remainder had a reamed-only hole (NCE) 22.6 mm in diameter.

To experimentally determine the through-thickness and surface stresses two methods were employed, namely, strain-gauge measurements, and bulk-stress measurements via a thermographic system. Both sets of measurements were made while the specimen was loaded in a standard servohydraulic test machine.

## 3.2 Strain-Gauge Stress Analysis

### 3.2.1 Testing Details

The four 10 mm and 35 mm thick specimens were strain-gauged down the bore of the hole to measure y and z strains with 120 ohm strip-gauges having a pitch of 2.03 mm. The 35 mm specimens were also strain-gauged on the surface to measure x and y strains, as per the schematic of Fig. 4. The x and z direction gauges had an active grid length of 0.7874 mm and width of 0.8128 mm, and the y direction gauges had an active grid length of 0.7874 mm and width of 1.778 mm. Strain readings were taken every 5 MPa, cycling from zero to 30 MPa to –30 MPa to zero (these applied stresses were based on gross area). Not all of the gauges were functioning correctly, therefore the data gained were limited. The data acquisition system used was a digital volt-meter type 3455A HP.

### 3.2.2 Calibration

As mentioned previously, a schematic of the location of the gauges is shown in Fig. 4. Due to the small difference in the positioning of the x and y strip gauges on the surface, and also the y and z strip gauges down the bore of the hole, interpolation of the strain readings was performed. Using these interpolated values, the stresses were calculated using the following equations:

on the surface;

$$\sigma_x = \frac{E(\varepsilon_x + \nu\varepsilon_y)}{1-\nu^2}, \qquad \sigma_y = \frac{E(\varepsilon_y + \nu\varepsilon_x)}{1-\nu^2}$$

down the bore of the hole;

$$\sigma_y = \frac{E(\varepsilon_y + \nu\varepsilon_z)}{1-\nu^2}, \qquad \sigma_z = \frac{E(\varepsilon_z + \nu\varepsilon_y)}{1-\nu^2}$$

where E = 73,084 MPa and $\nu = 0.33$

It should be noted that a strain-gauge reading is an average over the area of the grid of the gauge though it is usually taken, as at present, to be the value at the centre of the grid. Hence the stresses calculated as above, are also average values.

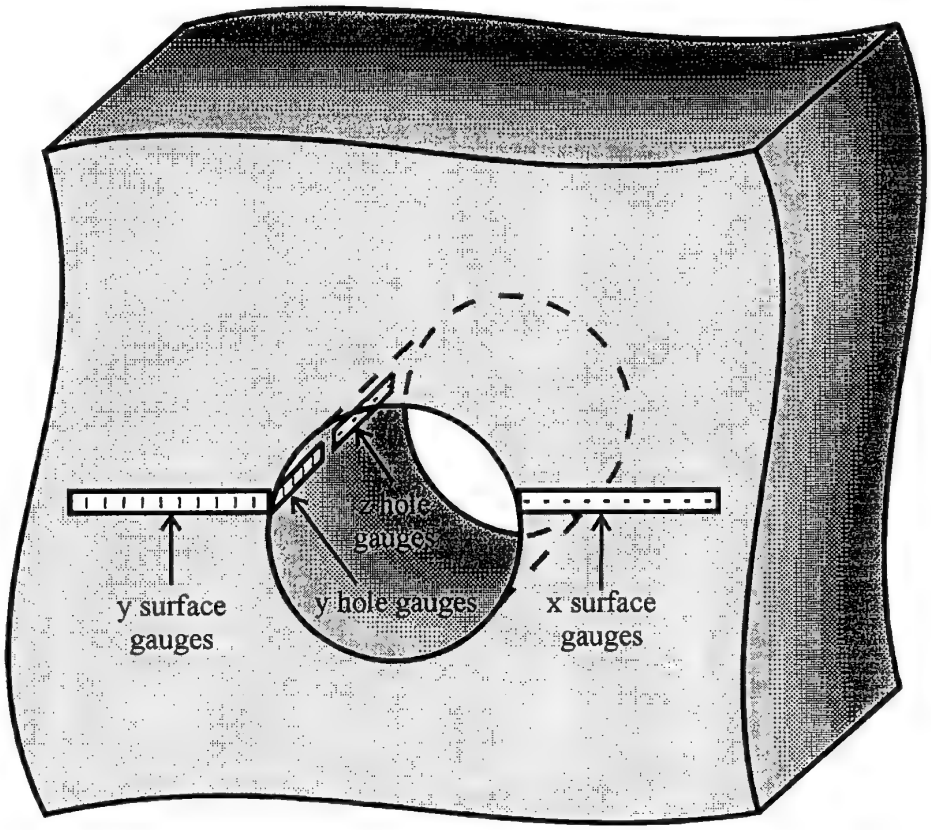


10 mm thick specimens

Hole
- 2 strain-gauges in y direction
- 3 strain-gauges in z direction

35 mm thick specimen

Surface
- 10 strain-gauges in x direction
- 10 strain-gauges in y direction

Hole
- 7 strain-gauges in y direction
- 7 strain-gauges in z direction

FIGURE 4. Schematic of strain-gauge locations

## 3.3 Thermoelastic Stress Analysis

### 3.3.1 Testing details

Thermographic measurements were taken of the bore of the hole and of the face of all six specimens (on the face opposite to the strain-gauges where appropriate). This was performed by the FAST system with the fatigue test machine applying an alternating stress of ±30 MPa at a frequency of 5 Hz. The resultant scans were 486 by 510 pixels in size. The system used in this experimental analysis is based on a real-time digital video processor and a focal-plane array thermal imager [7], which detects the minute changes in infra-red radiation caused by the thermoelastic effect. Changes in temperature of less than 0.01° C can be measured, with the specimens painted matt black to improve their emissivity. This system is able to deliver high resolution full-field thermoelastic stress scans of the specimen with a reduction in observation time of between one and two orders of magnitude [11] compared to the single sensor thermographic systems (such as SPATE) which create comparable stress plots by scanning one point at a time.

### 3.3.2 Calibration

As mentioned previously, the thermographic measurements for each specimen consisted of a surface scan and a scan down the bore of the hole. Two horizontal lines of data were extracted from the surface scans; one corresponding to the location of the x and y surface gauges (but on the opposite face), and the other, at location $y = 45$ mm. A line of data through the thickness of the specimen parallel to the z axis, corresponding to the location of the y and z hole strain-gauges (but on the opposite side) was obtained along the bore of the hole from the other scan. These line scans were adjusted for aberration.

#### 3.3.2.1 Surface Data

Various boundary conditions to model the mechanics of the fatigue-machine grips were implemented into the FE runs. From these results it was ascertained that within a vertical distance of 45 mm from the centre of the hole, the bulk stress distribution in the plate was unaffected by the grips. On the surface of the specimens the bulk stress was equal to $(\sigma_x + \sigma_y)$, as $\sigma_z = 0$. The plots of bulk stress for the numerical models (Fig. 5—which also includes the two-dimensional result for comparison) indicate that at this distance (of 45 mm) thickness effects are small. Thus the calibration location was selected as line $y = 45$ mm. The spatial-average numerical bulk-stress value at $y = 45$ mm was calculated for the specimen models of different thicknesses. The average uncalibrated bulk-stress value from the FAST data was then determined from the horizontal line scans at the calibration location for each specimen. The calibration factor (k) for each specimen was thus calculated as the ratio of the averages of numerical FE bulk stress to uncalibrated experimental bulk stress (refer to Table 3). The FAST data for each specimen were then multiplied by the corresponding factor k.

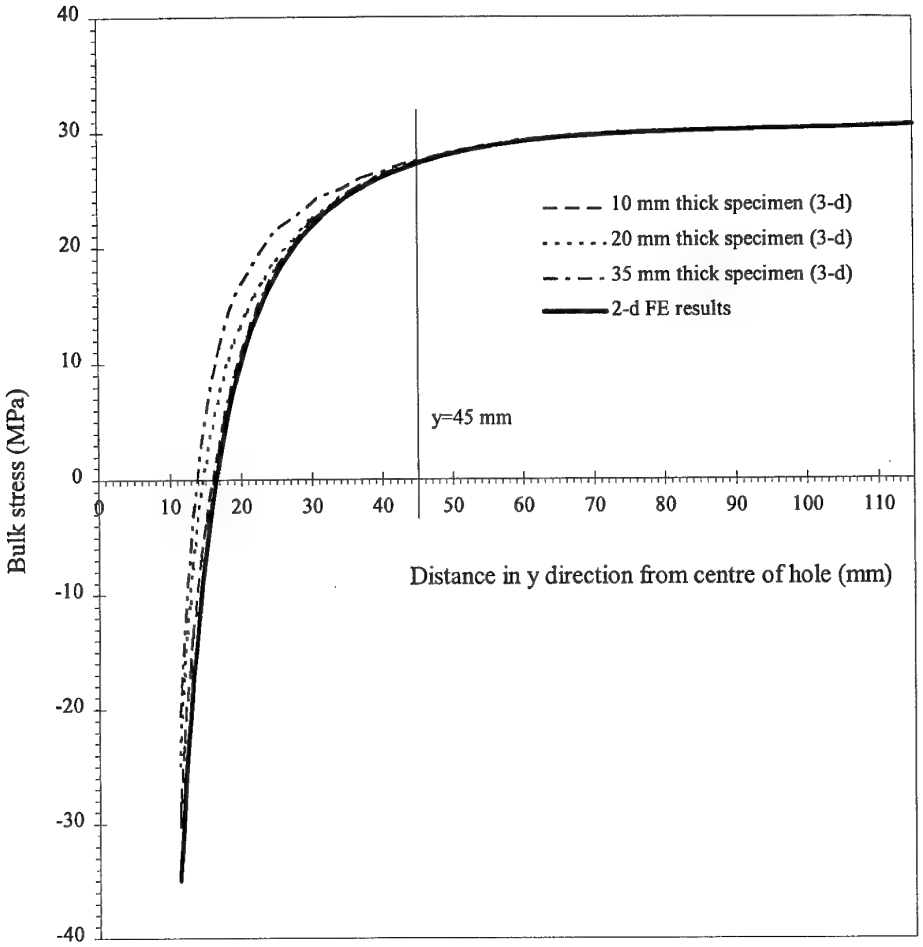


*Figure 5. Bulk-stresses parallel to the y axis at x=0, determined by FE, for specimens of different thickness*

*Table 3. Determination of calibration factors for FAST surface bulk stresses*

| Specimen | FAST uncalibrated average stress | FE spatial-average stress | Factor (k) |
|---|---|---|---|
| 10 mm, NCE | 47.56 | 30.21 | 0.635 |
| 10 mm, CE | 41.88 | 30.21* | 0.721 |
| 20 mm, NCE | 45.49 | 30.20 | 0.664 |
| 20 mm, CE | 41.23 | 30.20* | 0.733 |
| 35 mm, NCE | 50.23 | 30.24 | 0.602 |
| 35 mm, CE | 44.50 | 30.24* | 0.680 |

* These values are from a finite-element model of a NCE specimen

3.3.2.2 Through-Thickness Data

The uncalibrated bulk-stress data obtained from the through-thickness scans for each specimen were noisier than the surface data and a quadratic curve-fit was applied to each line scan. At this location down the bore of the hole the bulk stress is equal to $(\sigma_y + \sigma_z)$ as $\sigma_x = 0$. The calibration factor (k) was calculated by determining the spatial-average of the bulk-stress along a line in the z direction (at y = 0) as obtained by FE analysis, and dividing by the average of the corresponding curve-fitted uncalibrated FAST data (Table 4). The FAST data for each specimen were then multiplied by the corresponding factor k.

*Table 4. Determination of calibration factors for FAST through-thickness bulk stresses*

| Specimen | FAST uncalibrated average stress | FE spatial-average stress | Factor (k) |
|---|---|---|---|
| 10 mm, NCE | 101.0 | 99.46 | 0.985 |
| 10 mm, CE | 109.3 | 99.46* | 0.910 |
| 20 mm, NCE | 70.47 | 104.4 | 1.481 |
| 20 mm, CE | 56.40 | 104.4* | 1.851 |
| 35 mm, NCE | 76.19 | 109.6 | 1.439 |
| 35 mm, CE | 76.55 | 109.6* | 1.432 |

* These values are from a finite-element model of a NCE specimen

# 4. Results and Discussion

The majority of the experimental and numerical FE results are summarised in Figs. 6 to 11. Figures 6, 7 and 8 are normalized plots of the numerical and experimental surface data for the 10, 20 and 35 mm thick specimens respectively, where the bulk stresses are normalized by the applied stress. Figures 9, 10 and 11 are normalized plots of the numerical and experimental through-thickness data for the 10, 20 and 35 mm thick specimens respectively; the FAST data are represented by the associated curve-fit and standard deviation (SD). As with the surface data, the bulk stresses in Figs. 9–11 are normalized by the applied stress.

As mentioned in Section 2.2, the numerical models are of the non-cold-expanded specimens only, therefore the FE curve in the cold-expanded plots (Figs. (b) of Figs. 6-11) is of the non-cold-expanded (NCE) model of corresponding thickness. It should be noted that in the absence of a full elastic/plastic three-dimensional FE analysis of a cold-expanded hole and relevant strain-gauge data, calibration of the FAST data is complicated. Therefore, the results presented for the cold-expanded specimens show the *trends* of the data, not absolute values. These specimens were tested to experimentally investigate the effect of cold-expansion on the surface and through-thickness stresses at a hole.

## 4.1 Comparison of Experimental and Finite-Element Surface Data

From the surface lines of data in the x direction at y = 0 (Figs. 6–8) it can be seen that the experimental FAST data agree well with the numerical FE curves (in most cases). At the edges of the hole and plate, the FAST data points drop rapidly away from the numerical curves due to the nature of the FAST system; the data points are averaged by those around them. Hence, a sharp thermal representation at an edge cannot be attained. For the 10 and 20 mm thick specimens, the FAST data indicate that the bulk stress is higher in the NCE specimens. The FAST data of the 35 mm thick specimens tend to indicate the opposite, however, the strain-gauge readings closest to the hole for these specimens (Fig. 8) indicate that the bulk stress is lower for the cold-expanded specimen, as for the 10 and 20 mm thick specimens. However, due to a lack in consistency between the FE and FAST NCE data, there is not much confidence in drawing a conclusion from the FAST CE data. Apart from a few points, the strain-gauge measurements (available for the 35 mm thick specimens only) tend to follow the data of the FE model and the FAST data.

## 4.2 Comparison of Experimental and Finite-Element Through-Thickness Data

The experimental data gained from the through-thickness bulk-stress measurements are of poorer quality than desired. As mentioned earlier, the FAST data were noisy and had to be represented by a curve of best-fit. The SD which is indicated in Figs. 9-11 is quite large for the 35 mm thick specimens. On the whole, the general trends between the numerical and experimental data for the different thickness specimens are in agreement, ie, the maximum value of bulk stress tends to occur in the middle of the specimen ($z/t = 0$) and the minimum on the surface ($z/t = \pm 0.5$), however, the correlation between the magnitudes of the numerical and experimental data is a little unsatisfactory. Due to the nature of calibration it is not possible to make a profound statement regarding the comparison of the NCE and CE results.

## 4.3 General Trends of Finite-Element Through-Thickness Results

It can be seen from the numerical FE curves of Figs. 6–8 that as the thickness of the specimen increases, the maximum value of normalized bulk stress, which occurs at the edge of the hole, reduces. This is hence mirrored in the values of the normalized bulk stress at the surface in the corresponding through-thickness curves of Figs. 9-11. These figures also show that the maximum value of the normalized bulk stress occurs in the middle of the plate, increasing with increase in thickness. The $\sigma_z$ component of this bulk stress accounts for a small percentage of the total, the maximum value ranging from 13% to 56% of the remote applied stress ($\sigma_o$), whereas the maximum value of the $\sigma_y$ component ranges from 331% to 338% of $\sigma_o$. For the geometry of specimens tested the maximum $\sigma_z$ and $\sigma_y$ occurred in the middle of the plate. The maximum $\sigma_z$ value increased with increase in thickness, however, the maximum $\sigma_y$ value occurred in the 20 mm thick specimen.

The through-thickness FE data generated in the present work are summarised in Fig. 12, and are expressed as stress concentration factor versus normalized distance through the thickness. Two additional curves are plotted on this figure; an extra FE run with D/t = 8, and theoretical two-dimensional data from Peterson [9], both for the r and W dimensions of the specimens tested. As mentioned in Section 2.1, the numerical data of Fig. 12 are slightly higher than that of the published work, however, the trends are similar. From Fig. 12 it can be seen that for the large values of D/t, the gradient of the curves is small near the surface of the specimen, and the maximum values of $K_t$ occur in the centre of the specimen. The middle value of D/t (1.13) has a relatively higher value of maximum $K_t$ and the gradient of the curve near the surface is increased. The curve for the thickest specimen (ie, lowest D/t) has the largest gradient near the surface of the specimen, however, not the highest maximum $K_t$. Therefore, as the value of D/t is increased, the maximum value of $K_t$ in the centre of the specimen and the gradient of the curve near the surface of the specimen both reduce, tending towards a straight line, ie, the plane stress case. The variation in von Mises stress down the bore of the hole with ratio of D/t shows the same trend as the $K_t$ curves, however, it is more pronounced. Thus, as the thickness of the specimens increase, the maximum value of von Mises stress moves away from the centre of the plate towards the surface, which perhaps is an indicator of the location of fracture, as mentioned in [1]. Findings from theoretical papers also indicate that for ratios of $D/t \geq 4$ the assumption of plane stress is adequate, and the transition region from plane stress to plane strain occurs between D/t ratios of 0.5 to 4. Though not covering a full range of D/t ratios, the present numerical FE work confirms these conclusions.

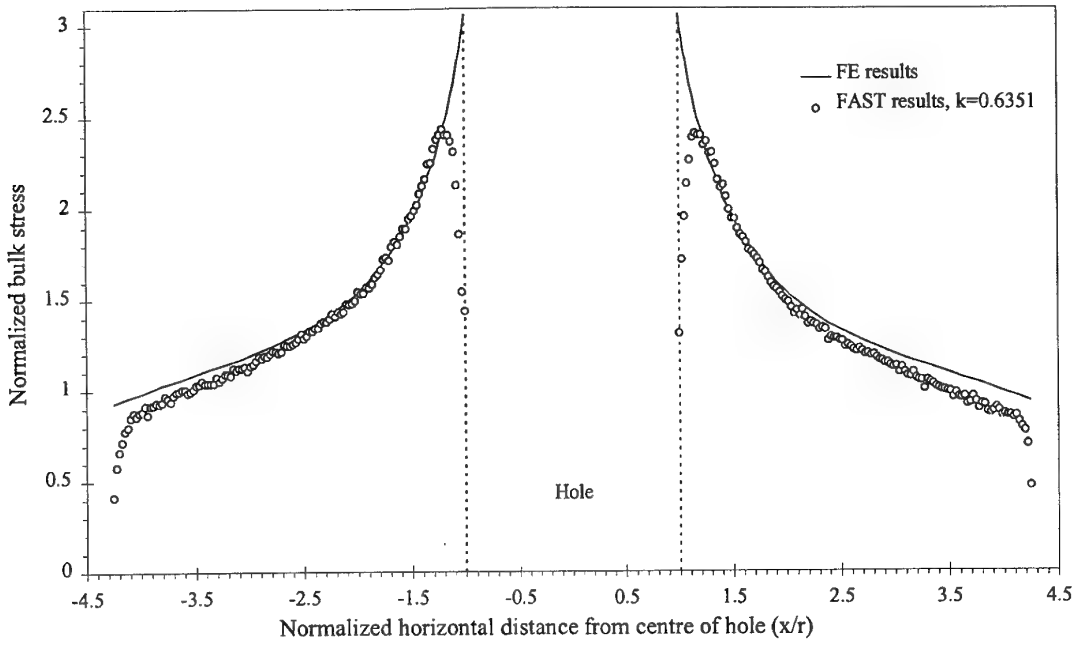


*(a) Non-cold-expanded specimen*

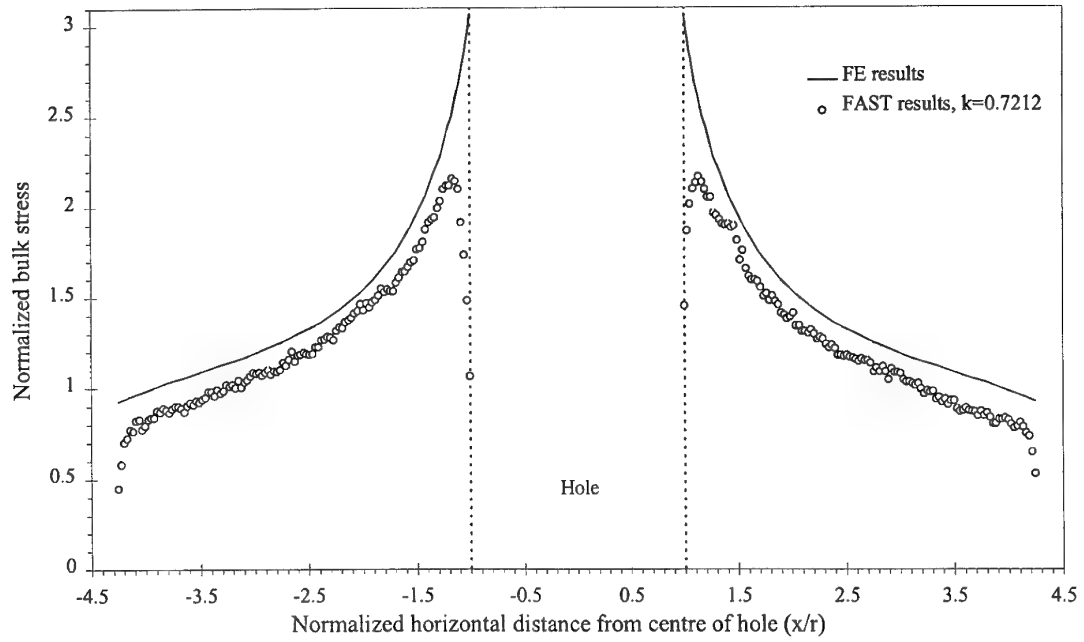


*(b) Cold-expanded specimen*

*Figure 6. Comparison of experimental and numerical normalized bulk-stresses parallel to the x axis at y=0 for 10 mm thick specimens*

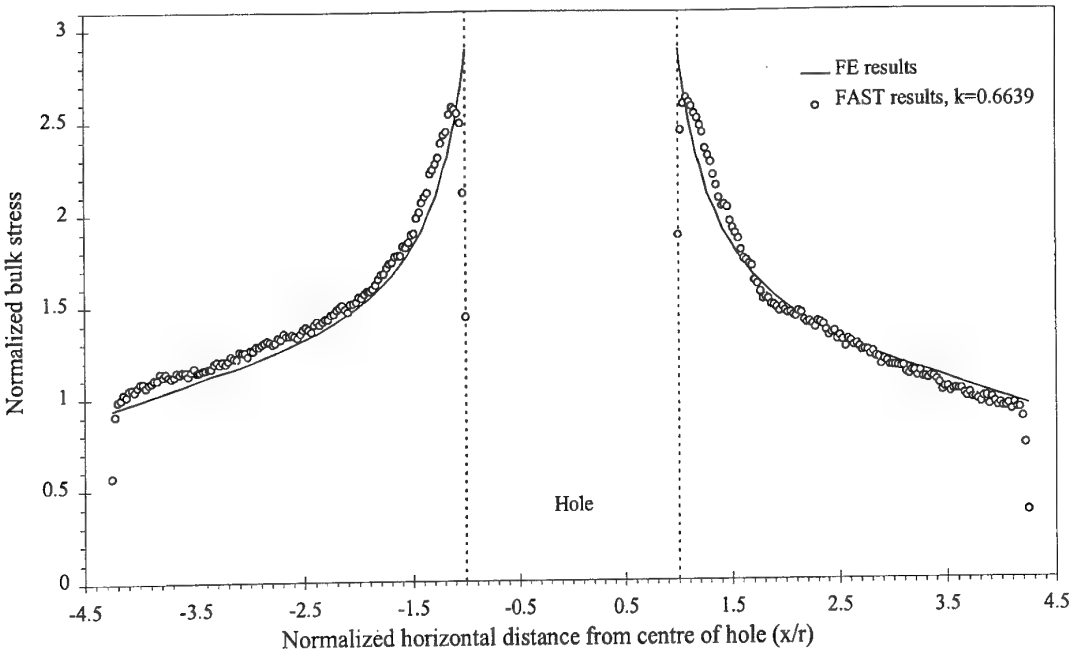


*(a) Non-cold-expanded specimen*

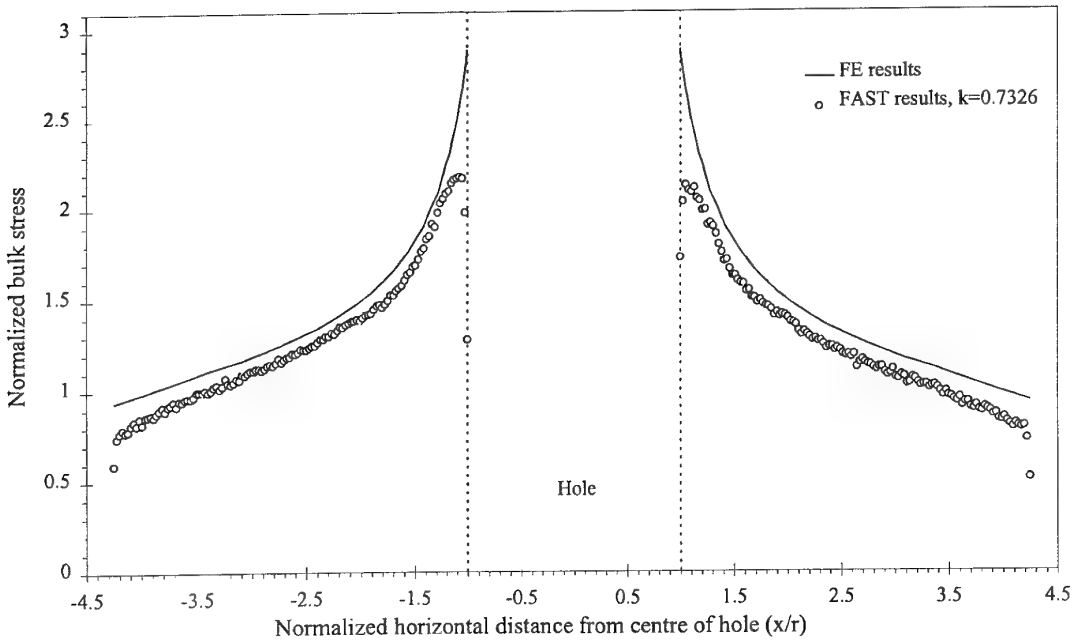


*(b) Cold-expanded specimen*

*Figure 7. Comparison of experimental and numerical normalized bulk-stresses parallel to the x axis at y=0 for 20 mm thick specimens*

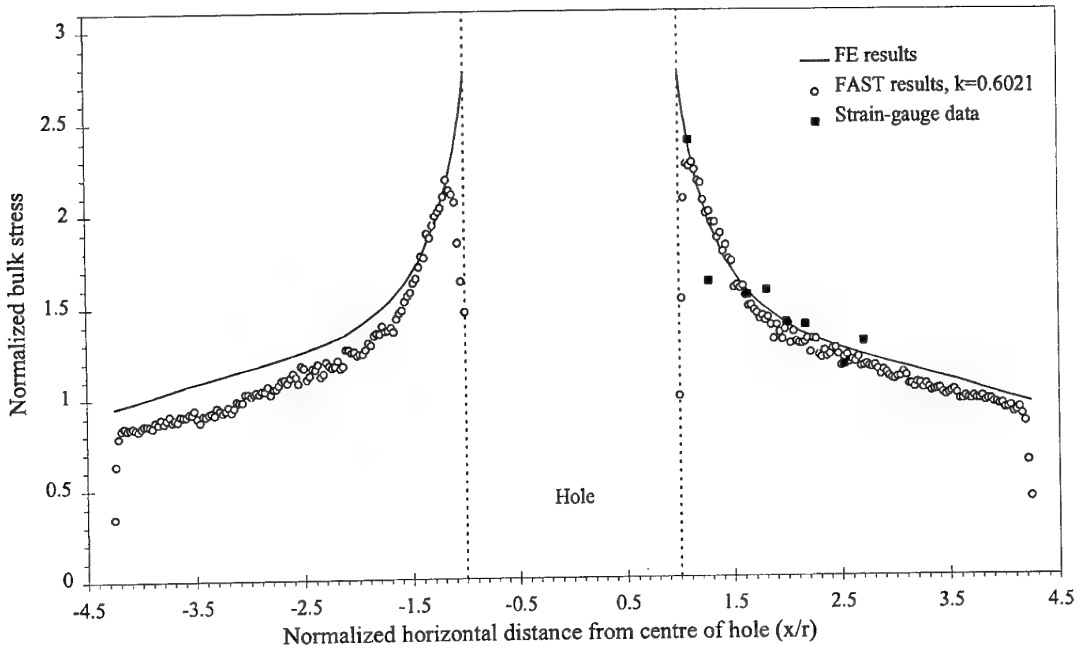


*(a) Non-cold-expanded specimen*

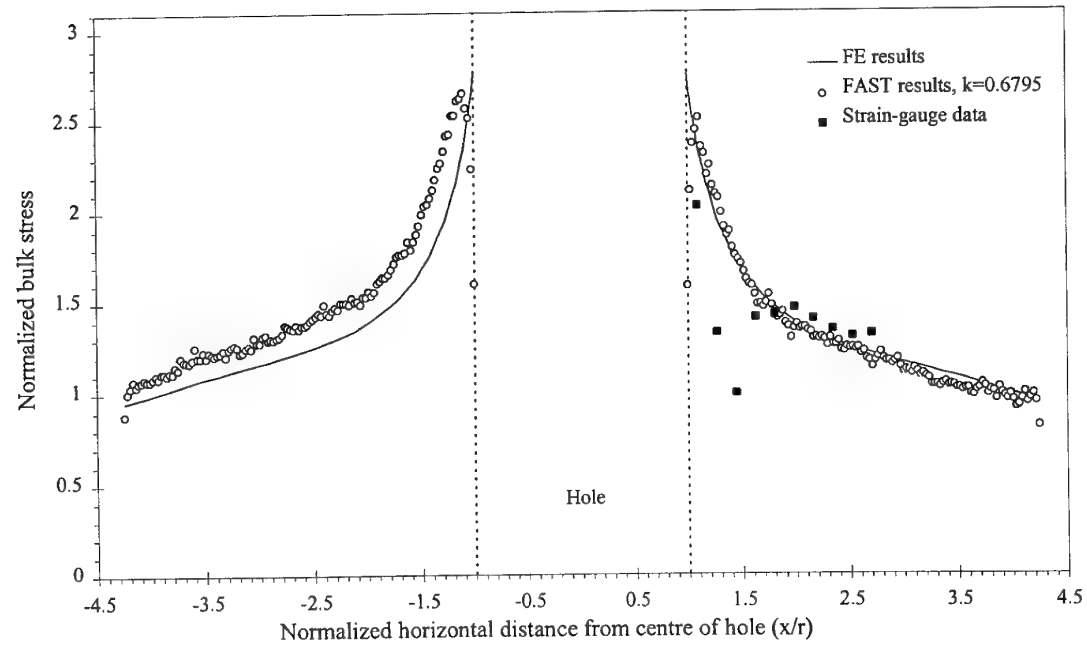


*(b) Cold-expanded specimen*

*Figure 8. Comparison of experimental and numerical normalized bulk-stresses parallel to the x axis at y=0 for 35 mm thick specimens*

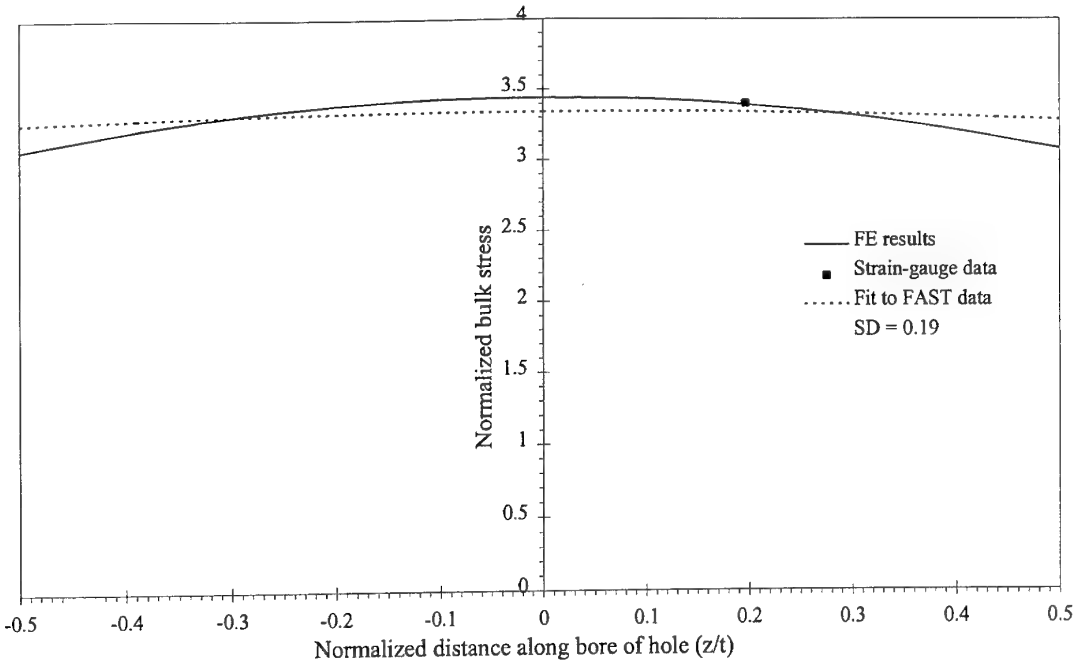


*(a) Non-cold-expanded specimen*

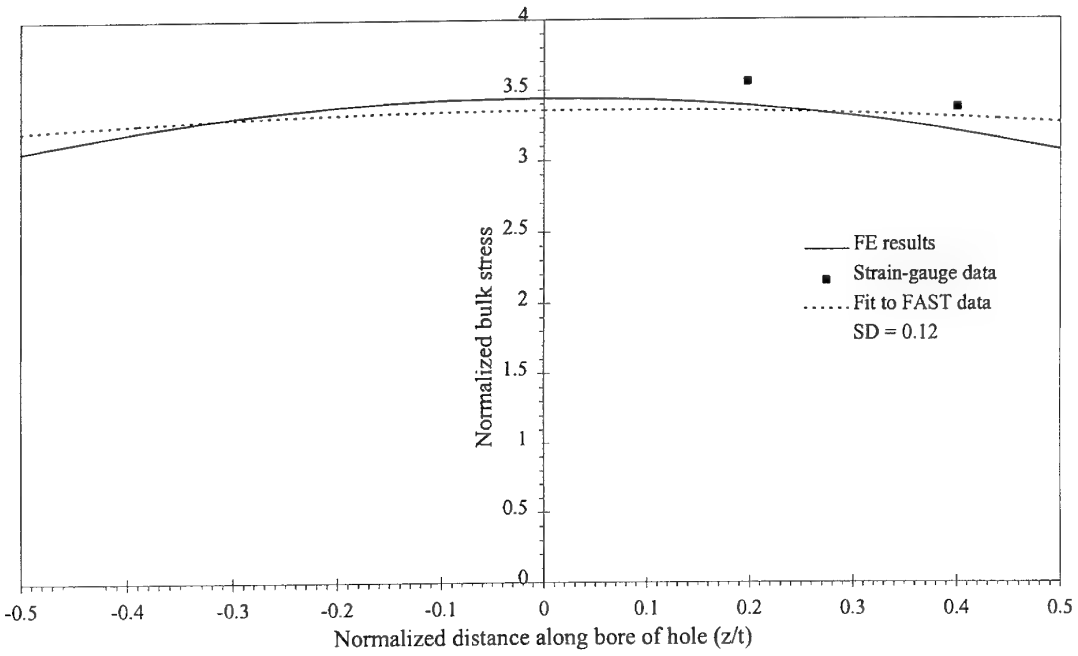


*(b) Cold-expanded specimen*

*Figure 9. Comparison of experimental and numerical normalized bulk-stresses along the bore of the hole for 10 mm thick specimens*

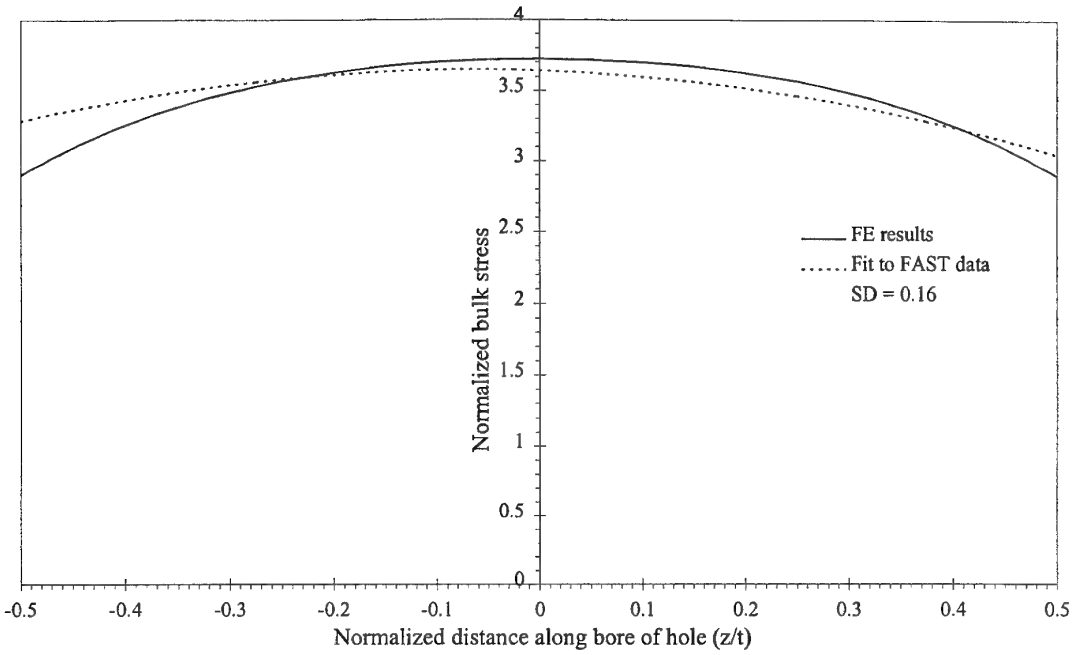


*(a) Non-cold-expanded specimen*

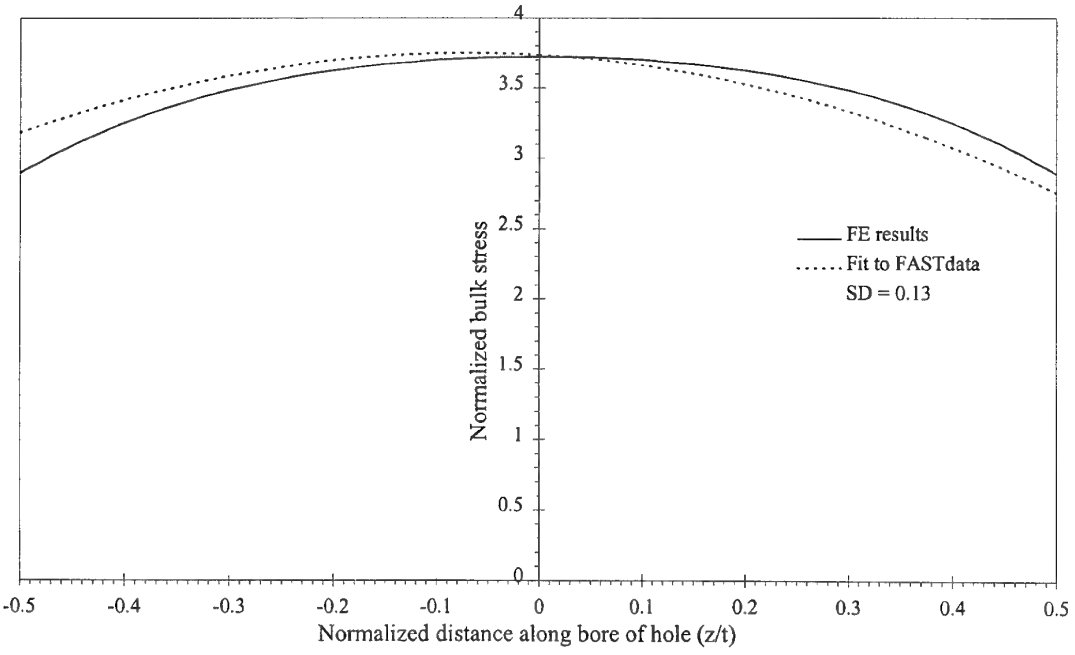


*(b) Cold-expanded specimen*

*Figure 10. Comparison of experimental and numerical normalized bulk-stresses along the bore of the hole for 20 mm thick specimens*

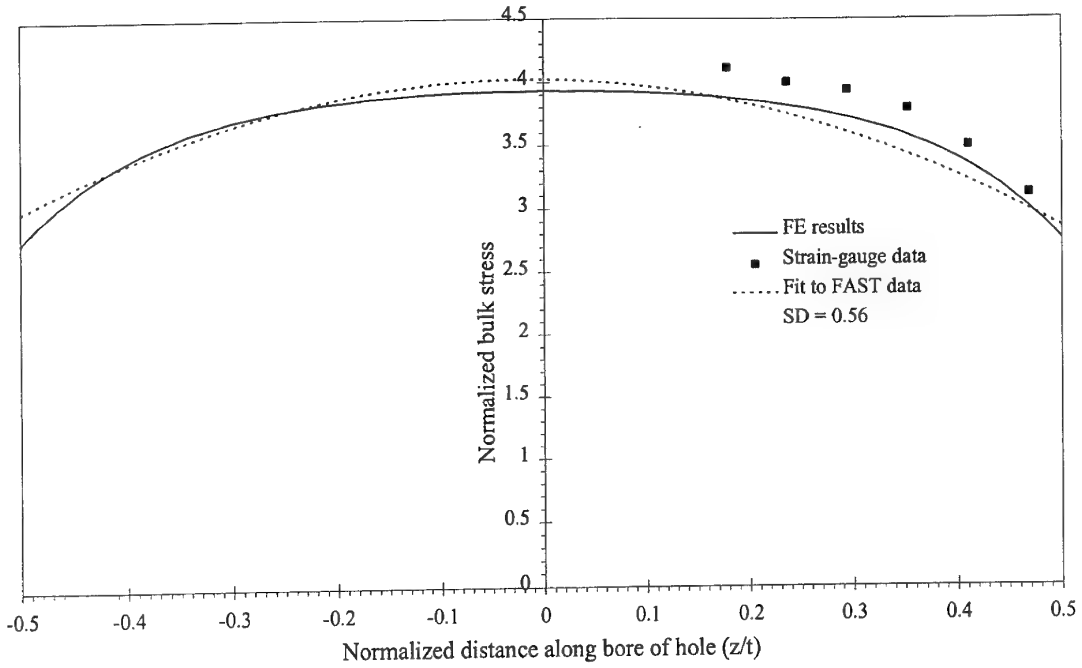


*(a) Non-cold-expanded specimen*

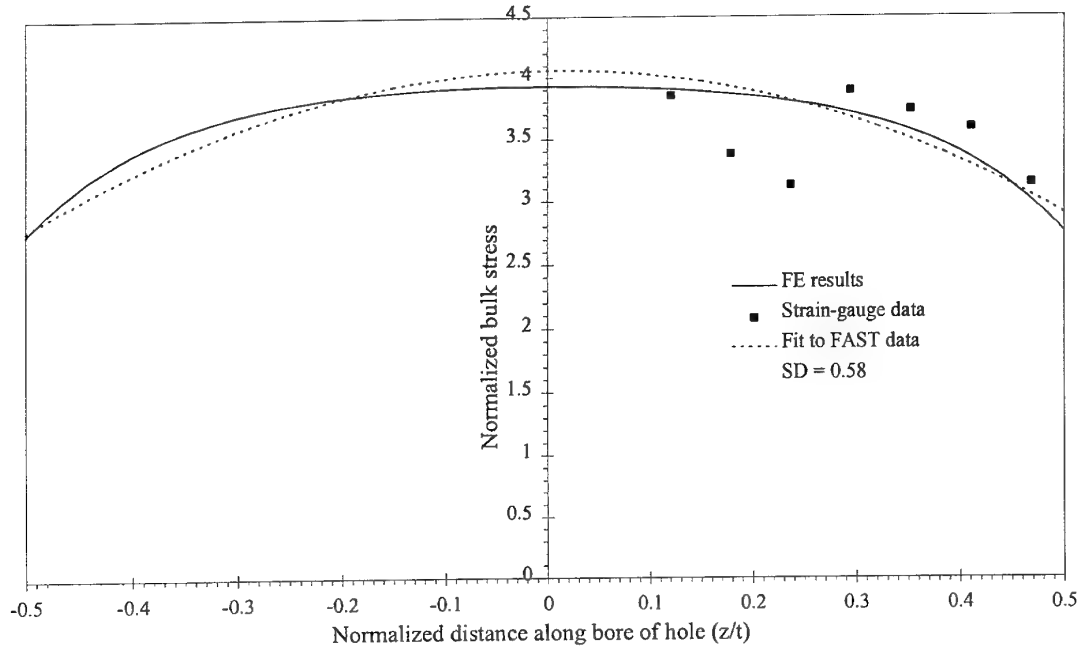


*(b) Cold-expanded specimen*

*Figure 11. Comparison of experimental and numerical normalized bulk-stresses along the bore of the hole for 35 mm thick specimens*

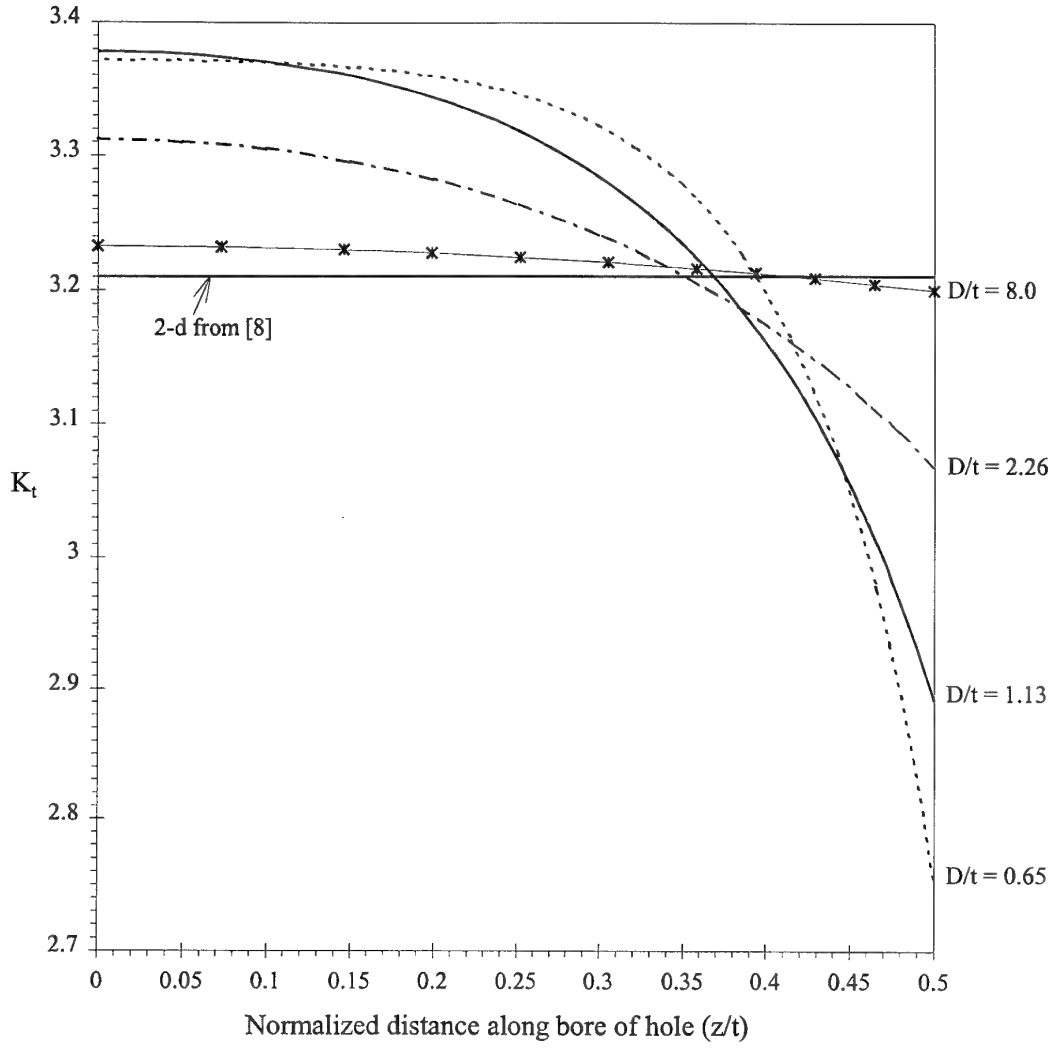


*Figure 12. Stress concentration factor along bore of hole at y=0 for various hole diameter to thickness ratios*

# 5. Conclusions

1. The elastic three-dimensional finite-element work undertaken validates the trends of the published FE and analytical studies, that as the thickness of a plate with a hole increases, the maximum stress concentration factor, which is in the middle of the plate, increases and the minimum value of stress concentration factor, which is at the surface of the plate, decreases. Thus, care must be taken in engineering calculations for thick plates with holes—the use of a two-dimensional handbook stress concentration factor may be too conservative at the surface, but unconservative at mid-thickness.

2. The three-dimensional finite-element analyses have indicated that $\sigma_z$ accounts for only a small percentage of the bulk stress through the thickness of the specimen compared to $\sigma_y$. The maximum value of $\sigma_z$ ranged from 13% to 56% of the remote applied stress, whereas the maximum value of the $\sigma_y$ component ranged from 331% to 338% of the remote applied stress. For all thicknesses of specimen tested (10, 20 and 35 mm) the maximum of $\sigma_z$ and $\sigma_y$ occurred in the middle of the plate—the maximum $\sigma_z$ value increased with increase in thickness, however, the maximum $\sigma_y$ value occurred in the 20 mm thick specimen.

3. The experimental FAST data compared well with the numerical FE work for the surface of the specimens. The corresponding through-thickness data were not as clearly in accordance. Apart from a few points, the strain-gauge trends appeared to agree with the FE models and the thermoelastic data. However, it would seem that for better experimental results for the through-thickness work, either smaller and more reliable strain-gauges and/or FAST measurements with reduced noise are needed.

# 6. Acknowledgements

The author would like to thank Drs Finney and Heller for their guidance and contributions towards this report. The author also wishes to thank Mr Ferrarotto for the strain-gauging and data acquisition, Drs Wong and Ryall, Ms Cox and Mr Rowlands for the experimental FAST measurements, and Messrs Absolom and Ryan for running the test machine. Mr Cheung's work in creating and running the NASTRAN models was greatly appreciated.

# 7. References


1. ES Folias & JJ Wang, "On the three-dimensional stress field around a circular hole in a plate of arbitrary thickness", *Computational Mechanics Vol. 6 No. 3*, 1990 pp 379-391.
2. CK Youngdahl & E Sternberg, "Three-dimensional stress concentration around a cylindrical hole in a semi-infinite elastic body", *Journal of Applied Mechanics Vol. 33*, 1966 pp 855-865.
3. ES Folias, "The 3D stress field at the intersection of a hole and a free surface", *International Journal of Fracture Vol. 35*, 1987 pp 187-194.
4. E Sternberg & MA Sadowsky, "Three-dimensional solution for the stress concentration around a circular hole in a plate of arbitrary thickness", *Journal of Applied Mechanics Vol. 16*, 1949 pp 27-38.
5. FE Penado & ES Folias, "The three-dimensional stress field around a cylindrical inclusion in a plate of arbitrary thickness", *International Journal of Fracture Vol. 39*, 1989 pp 129-146.
6. KN Shivakumar & JC Newman, Jr., "Stress Concentrations for straight-shank and countersunk holes in plates subjected to tension, bending and pin loading", *NASA technical paper 3192*, 1992.
7. TG Ryall & AK Wong, "Design of a focal plane array thermographic system for stress analysis", *Experimental Mechanics Vol. 35 No. 2*, 1995 pp 144-147.
8. AKH Cheung, Private communication re. NASTRAN finite-element models, CRC-AS, June 1995.
9. RE Peterson, "Stress concentration factors", published by John Wiley & Sons, 1974 Figure 88, p 152.
10. JL Phillips, "Fatigue improvement by sleeve cold working", *SAE Paper no. 730905*, 1973.
11. AK Wong & TG Ryall, "Performance of the FAST system for stress analysis", *Experimental Mechanics Vol. 35 No. 2*, 1995 pp 148-152.

Appendix A

# PAFEC data file for 10 mm thick specimen

```
C PAFEC 3D GEOMETRY FOR A HOLE IN A PLATE
C MODEL IS 1/8 SYMMETRIC, MATERIAL: AL ALLOY 2214-T651
C THICKNESS: 10 mm, HOLE DIAMETER: 22.6 mm
C
CONTROL
FULL.CONTROL
PHASE=1
PHASE=2
PHASE=4
PHASE=6
PHASE=7
PHASE=9
CONTROL.END
C
NODES
NODE.NUMBER     X               Y               Z
1               0               11.3            0
2               4.324322786     10.43983872     0
3               7.990306628     7.990306628     0
4               10.4398387      4.324322786     0
5               11.3            0               0
6               20.0            0               0
7               48.0            0               0
8               0               20.0            0
9               20.0            20.0            0
10              48.0            20.0            0
11              0               115.0           0
12              48.0            115.0           0
13              20.0            115.0           0
14              0               0               0
15              0               11.3            5.0
16              4.324322786     10.43983872     5.0
17              7.990306628     7.990306628     5.0
18              10.4398387      4.324322786     5.0
19              11.3            0               5.0
20              20.0            0               5.0
21              48.0            0               5.0
22              0               20.0            5.0
23              20.0            20.0            5.0
24              48.0            20.0            5.0
25              0               115.0           5.0
26              48.0            115.0           5.0
27              20.0            115.0           5.0
28              0               0               5.0
C END OF NODES
C
C BRICK CONFIGURATION
PAFBLOCKS
PROPERTIES=11
ELEM=37110
TYPE=1
BLOCK   GROUP   N1      N2      N5      TOPOLOGY
1       1       1       4       6       1,3,15,17,8,9,22,23,2,0,0,16
2       2       2       4       6       3,5,17,19,9,6,23,20,4,0,0,18
3       3       3       7       6       6,7,20,21,9,10,23,24
4       4       1       5       6       8,9,22,23,11,13,25,27
5       5       3       5       6       9,10,23,24,13,12,27,26
C
C END OF PAFBLOCKS
```

```
C
MESH
REFERENCE        SPACING.LIST
1                5
2                1,1,1,1,1,1,1,1,1,.5,.5
3                1,1,2,2,4,4
4                .45,.45,1,1,2,2,2,2
5                2,3,5,5,5,5,5,5,5,5,10,10,10,10,10
6                0.4,0.4,0.6,0.6,1,1,1
7                .5,.5,1,1,1,1,1,1,1,1,1
C
C END OF MESH
C
MATERIAL
MATERIAL.NUMBER          E          NU
11                       73084.5    0.33
C
C END OF MATERIAL
C
RESTRAINTS
NODE.NUMBER      PLANE   DIRECTION
1                1       1
5                2       2
15               3       3
C
C END OF RESTRAINTS
C
SURFACE.FOR.PRESSURE
PRESSURE.VALUE   NODE    PLANE
-30.0            11      2
C
C END OF PRESSURE
C
END.OF.DATA
```

Effect of plate thickness on the in-plane and through-thickness stresses at a hole
R.L. Evans

**AUSTRALIA**

**TASK SPONSOR: AIR OIC ASI-LSA**

**DEFENCE ORGANISATION**

**Defence Science and Technology Organisation**
Chief Defence Scientist
FAS Science Policy
AS Science Corporate Management
AS Science and Industry Interaction
} shared copy
Counsellor Defence Science, London (Doc Data Sheet only)
Counsellor Defence Science, Washington
Scientific Adviser to MRDC Thailand (Doc Data Sheet Only)
Senior Defence Scientific Adviser/Scientific Adviser Policy and Command (shared copy)
Navy Scientific Adviser (3 copies Doc Data Sheet and 1 copy distribution list)
Scientific Adviser - Army (Doc Data Sheet and distribution list only)
Air Force Scientific Adviser
Director Trials

**Aeronautical and Maritime Research Laboratory**
Director
Chief of Airframes and Engines Division
Research Leader Fracture Mechanics
M. Heller
T.G. Ryall
A.K. Wong
Author: R.L. Evans

**DSTO Library**
Library Fishermens Bend
Library Maribyrnong
Library DSTOS ( 2 copies)
Library, MOD, Pyrmont (Doc Data sheet)

**Defence Central**
OIC TRS, Defence Central Library
Officer in Charge, Document Exchange Centre (DEC), 1 copy
DEC requires the following copies of public release reports to meet exchange agreements under its management:
US Defence Technical Information Centre, 2 copies
UK Defence Research Information Centre, 2 copies
Canada Defence Scientific Information Service, 1 copy
NZ Defence Information Centre, 1 copy
National Library of Australia, 1 copy
Defence Intelligence Organisation
Library, Defence Signals Directorate (Doc Data Sheet only)

**Air Force**
Director General Force Development (Air)

**Army**

Director General Force Development (Land), (Doc Data Sheet)
ABCA Office, G-1-34, Russell Offices, Canberra (4 copies)

**Navy**

Director General Force Development (Sea), (Doc Data Sheet)

**UNIVERSITIES AND COLLEGES**

Australian Defence Force Academy
Library
Head of Aerospace and Mechanical Engineering
Deakin
Serials Section (M list) Library, Geelong, 3217
Monash
Senior Librarian, Hargrave Library
Head Materials Engineering
Flinders University
Sydney
Engineering Library
Head School of Mechanical & Mechatronic Engineering
Head School of Aeronautical Engineering
Melbourne
Engineering Library
NSW
Head, Mechanical Engineering
Tasmania
Engineering Library
Western Australia
Head Mechanical Engineering
RMIT
Library

**OTHER ORGANISATIONS**

NASA (Canberra)
AGPS
ASTA Engineering, Document Control Office
Hawker de Havilland Aust Pty Ltd, Bankstown, Library
BHP Melbourne Research Laboratories

**ABSTRACTING AND INFORMATION ORGANISATIONS**

INSPEC: Acquisitions Section Institution of Electrical Engineers
Library, Chemical Abstracts Reference Service
Engineering Societies Library, US
American Society for Metals
Documents Librarian, The Center for Research Libraries, US

**INFORMATION EXCHANGE AGREEMENT PARTNERS**

Acquisitions Unit, Science Reference and Information Service, UK
Library - Exchange Desk, National Institute of Standards and Technology, US
National Aerospace Laboratory, Japan
National Aerospace Laboratory, Netherlands

SPARES (10 copies)

**DEFENCE SCIENCE AND TECHNOLOGY ORGANISATION**
**DOCUMENT CONTROL DATA**

1. PRIVACY MARKING/CAVEAT (OF DOCUMENT)

2. TITLE

Effect of Plate Thickness on the In-Plane and Through-Thickness Stresses at a Hole

3. SECURITY CLASSIFICATION (FOR UNCLASSIFIED REPORTS THAT ARE LIMITED RELEASE USE (L) NEXT TO DOCUMENT CLASSIFICATION)

| | |
|---|---|
| Document | (U) |
| Title | (U) |
| Abstract | (U) |

4. AUTHOR(S)

R.L. Evans

5. CORPORATE AUTHOR

Aeronautical and Maritime Research Laboratory
PO Box 4331
Melbourne Vic 3001

| 6a. DSTO NUMBER | 6b. AR NUMBER | 6c. TYPE OF REPORT | 7. DOCUMENT DATE |
|---|---|---|---|
| DSTO-TR-0330 | AR-009-683 | Technical Report | April 1996 |

| 8. FILE NUMBER | 9. TASK NUMBER | 10. TASK SPONSOR | 11. NO. OF PAGES | 12. NO. OF REFERENCES |
|---|---|---|---|---|
| M1/009/110 | AIR 21-227C | AIR | 31 | 11 |

13. DOWNGRADING/DELIMITING INSTRUCTIONS

To be reviewed April, 1999.

14. RELEASE AUTHORITY

Chief, Airframes and Engines Division

15. SECONDARY RELEASE STATEMENT OF THIS DOCUMENT

Approved for public release

OVERSEAS ENQUIRIES OUTSIDE STATED LIMITATIONS SHOULD BE REFERRED THROUGH DOCUMENT EXCHANGE CENTRE, DIS NETWORK OFFICE, DEPT OF DEFENCE, CAMPBELL PARK OFFICES, CANBERRA ACT 2600

16. DELIBERATE ANNOUNCEMENT

No limitations

17. CASUAL ANNOUNCEMENT Yes

18. DEFTEST DESCRIPTORS

Stress; Aluminium alloys; Hole stresses

19. ABSTRACT

A combined experimental and numerical study has been carried out to examine the influence of thickness on the surface and through-thickness stress distributions of aluminium alloy specimens with central holes. Thermographic and strain-gauge measurements were made on several thicknesses of specimens, the central holes of which were either reamed or cold-expanded by 3.6%. The experimental results were compared with those from numerical analyses of the specimens by three-dimensional finite-element modelling.